2026 EAGE ANNUAL
87TH CONFERENCE & EXHIBITION
ABERDEEN | UK

3D extended receiver full waveform inversion: complexity analysis and OBC field data application

M. Benziane[1], R. Brossier[2], L. Métivier[2,3]

[1] Mines Paris PSL Centre for statistics and images (STIM); [2] Univ Grenoble Alpes ISTerre; [3] Univ Grenoble Alpes CNRS LJK

Summary

Full Waveform Inversion (FWI) is prone to cycle-skipping when the initial model lacks kinematic accuracy. To mitigate this in 3D large-scale problems, we propose a time-dependent receiver extension strategy. This method treats receivers positions as additional degrees of freedom, allowing them to move during the simulation to fit data in inaccurate velocity models. We solve the resulting non-convex optimization subproblem using an efficient dynamic-programming approach. We demonstrate the method effectiveness on the Valhall Life of Field Seismic (LoFS) OBC dataset. Unlike conventional FWI, our approach successfully reconstructs shallow low-velocity channels and deep reflectors starting from a smoothed tomographic model. Furthermore, we provide a complexity analysis showing that extended receiver FWI scales with the maximum frequency ω as $O(\omega^2)$, whereas the 3D FWI simulation scales as $O(\omega^4)$. This confirms that the computational overhead of the extension becomes negligible as frequency increases, offering a robust and scalable solution for 3D large scale applications.

3D extended receiver full waveform inversion: complexity analysis and OBC field data application

Introduction

Full Waveform Inversion (FWI) has become the industry standard for high-resolution subsurface imaging. It is a data-fitting procedure where the fit between the observed data and the synthetic data is improved iteratively, using gradient-based optimization techniques. The FWI misfit function (conventionally the least-squares) is non-convex, making gradient-based optimization approaches highly dependent on the initial model: an initial model that does not honor the kinematics of the seismic data, up to half a dominant period, leads FWI to converge to a local minimum. This is manifested as a phase ambiguity, which is called cycle-skipping in the literature (Virieux and Operto, 2009).

Many techniques have been proposed to circumvent the cycle-skipping issue, ranging from multi-scale approaches (Bunks et al., 1995) to misfit function modification (e.g. Warner and Guasch, 2016; Métivier et al., 2018) and extension strategies (Symes, 2008; Métivier and Brossier, 2022; Operto et al., 2023). The method presented in this study is an extension method. An extension method introduces additional degrees of freedom to the FWI problem, which mitigates the non-convexity by effectively explaining the data in inaccurate velocity models. Receiver extension, first introduced by Métivier and Brossier (2022), makes the receiver position a free parameter and includes it in the FWI optimization. In previous works, we have improved the method by making the receiver position depend on the simulation time (e.g. Benziane et al., 2025b). Time-dependent receiver extension generates enough degrees of freedom to align multi-arrival data in inaccurate initial models, thereby alleviating cycle-skipping.

In the present study, we show for the first time an application of this method to a 3D field OBC data from the North Sea. Lastly, we provide a complexity analysis and discuss the scalability of the method for large-scale 3D applications.

Method

The extended-receiver FWI misfit function is given by

$$\min_{m,\Delta x(t)} f(m,\Delta x(t)) = \min_{m,\Delta x(t)} \frac{1}{2}\sum_{r=1}^{N_r}\int_0^T |d_{cal,r}[m,\Delta x_r(t)](x_r,t) - d_{obs,r}(x_r,t)|^2 dt + \alpha \sum_{r=1}^{N_r} \mathscr{P}_1[\Delta x_r(t)] + \beta \sum_{r=1}^{N_r} \mathscr{P}_2[\Delta \dot{x}_r(t)]. \tag{1}$$

The misfit function shown in Equation (1) is bivariate, where m represents the subsurface parameters and $\Delta x(t)$ is the receiver relocalization (our added degree of freedom). N_r and r are the number of receivers and receiver index, respectively. The misfit function is shown for a single source, extension to multiple sources is achieved by a simple summation. The first term on the right-hand side is the data misfit between the observed data and the extended data; the latter is obtained at extended receiver time-dependent positions. The second and third terms on the right-hand side are penalty terms for the receiver position and velocity, respectively.

The extended data are extracted from the synthetic wavefield as follows

$$d_{cal,r}[m,\Delta x_r(t)] = R_r[\Delta x_r(t)]u[m] = \int_\Omega \delta(x-(x_r+\Delta x_r(t)))u[m]dx, \tag{2}$$

where u is the synthetic wavefield computed using a wave equation, and R_r is the extended restriction operation which extracts the wavefield at extended receiver positions $x_r + \Delta x_r(t)$.

The misfit function of Equation (1) is minimized using a nested approach (Métivier and Brossier, 2022), where the outer problem is the FWI optimization over the subsurface parameters m, while the inner problem corresponds to the receiver extension subproblem, which is non-convex. In previous work, we devised an efficient strategy (Benziane et al., 2025a), which uses a tabulated dynamic-programming approach, reminiscent of the dynamic time warping algorithm of Hale (2013).

In essence, the algorithm tabulates the point-wise cost for all possible receiver spatial shifts and all time steps. The cost is then accumulated, and recursion is performed to reconstruct the time-dependent receiver relocalization.

The 3D implementation of the method relies on a parsimonious parametrization: the receivers are allowed to move solely along the line defined by the source and receiver positions. In other words, a receiver can only move towards or away from the source. This parametrization choice is crucial: first, it allows keeping the receiver extension subproblem 1D, which is a requirement for our dynamic programming solver; second, this choice reduces the position ambiguity, acting as spatial regularization.

OBC field data application

To test the proposed method on field data, we use the dataset from the Valhall Life of Field Seismic (LoFS) project (Barkved et al., 2003). The data were acquired in the southern part of the Norwegian North Sea; this is a site for permanent seismic monitoring and has become a calibrated benchmark for testing advanced seismic imaging algorithms due to its well-documented geological complexities (e.g. Métivier et al., 2025).

In this case study, we use an initial model obtained by smoothing the reflection travel-time tomography model, using a Gaussian kernel with a 1000 m correlation length (Figure 1). The inversion is started directly in the 2-7 Hz frequency band. These choices are made in an effort to simplify the standard FWI workflow, and to reduce the necessity of a high quality initial model.

We perform 50 iterations of conventional FWI, static receiver extension, and time-dependent receiver extension, using the visco-acoustic wave equation with Vertical Transverse Isotropy (VTI). Conventional FWI is unable to correctly reconstruct the velocity model, introducing low-velocity artifacts, particularly in the shallow parts (Figure 2). The reconstructed model obtained with static extended receiver FWI shows significant improvement (Figure 3). The low velocity anomaly is resolved, as well as the shallow glacial sand channels. The model obtained with the time-dependent approach (Figure 4) exhibits further improvements: the shallow section is better resolved, and the deep reflectors (between 1.5 and 3 km) are sharper and more continuous. This is corroborated by the well logs (Figure 5): the velocity profiles retrieved by both extension approaches generally follow the well log trend, with the time-dependent approach providing a better fit in the shallow section.

The computational overhead of the static approach is 3%, which is negligible (Table 1), while for the time-dependent approach the overhead is 17%, which remains computationally manageable.

Complexity analysis

We analyze the computational cost as a function of the maximum frequency ω. For conventional time-domain FWI, the grid spacing scales as $h \propto 1/\omega$, and the time step as $\Delta t \propto h \propto 1/\omega$ (CFL condition).

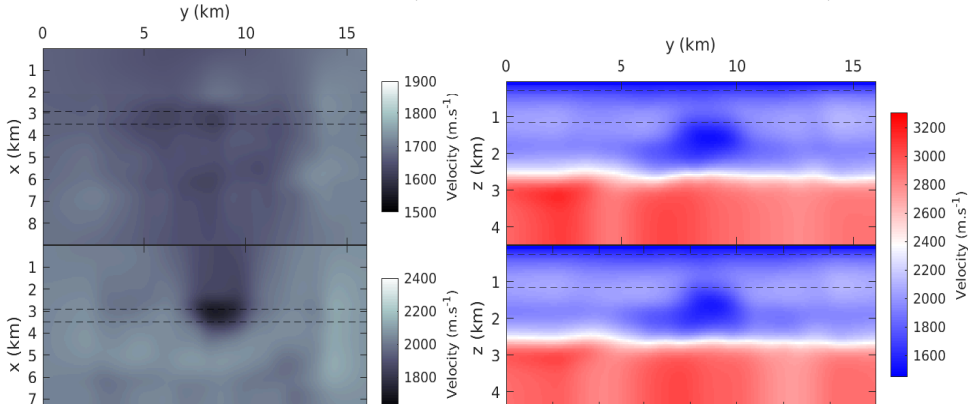

Figure 1: *Initial model used for all the FWI runs shown herein. The left panel shows the horizontal slices, the position of which is indicated on the right panel. The right panel shows a vertical slice whose position is shown in the left panel.*

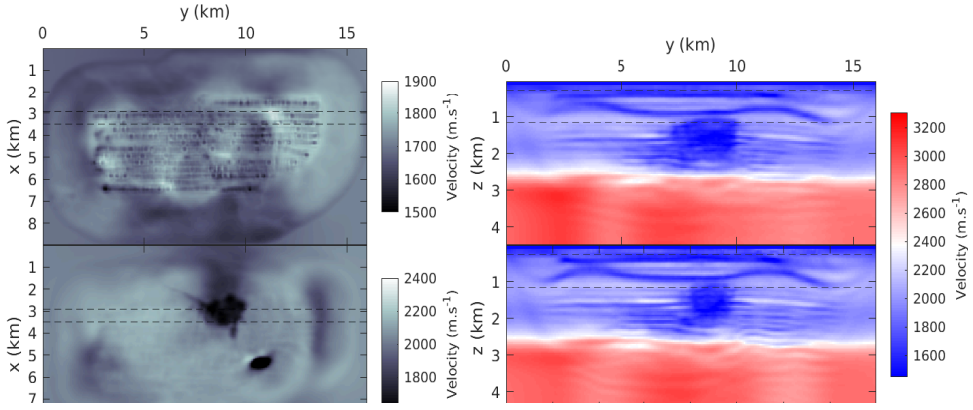

Figure 2: *Reconstructed model obtained after 50 iterations of conventional FWI.*

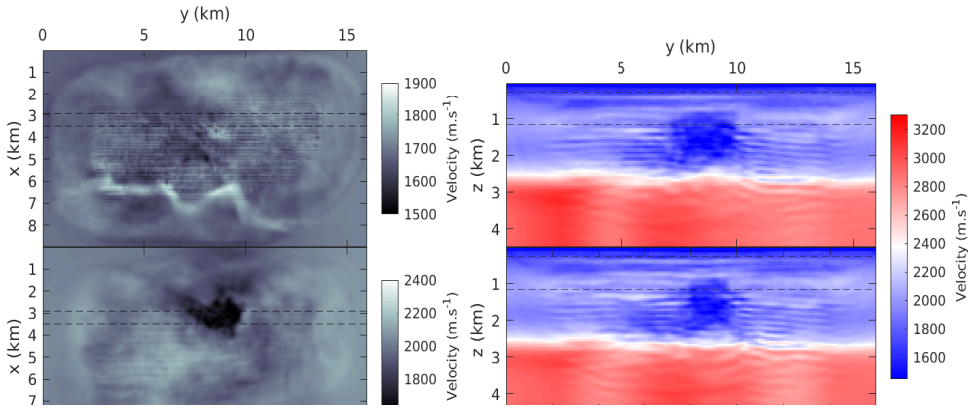

Figure 3: *Reconstructed model obtained after 50 iterations of static extended receiver FWI.*

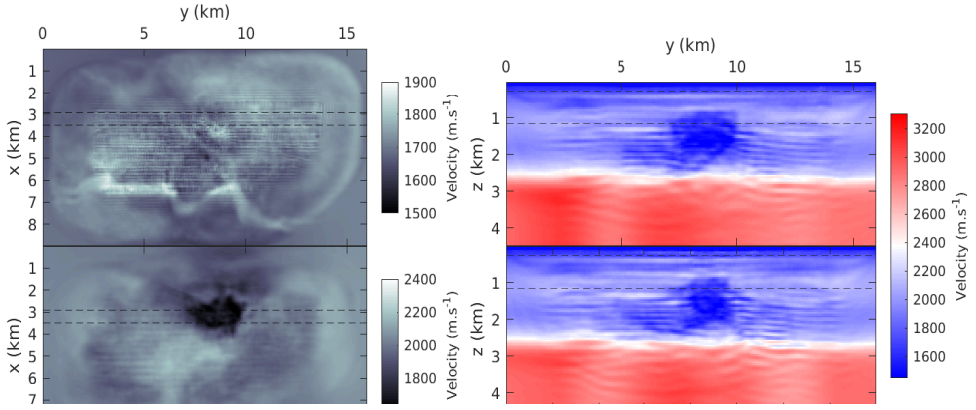

Figure 4: *Reconstructed model obtained after 50 iterations of time-dependent extended receiver FWI.*

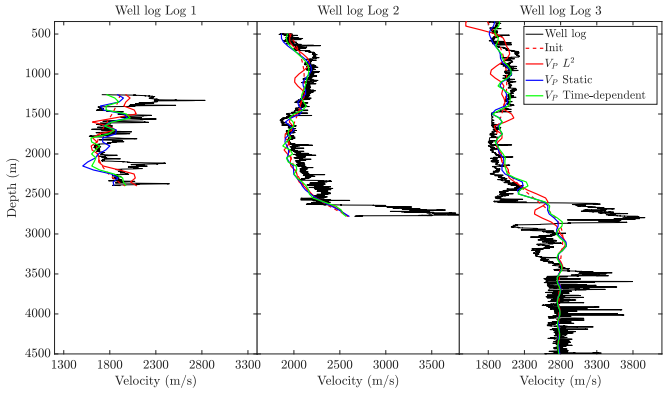

Figure 5: *Well logs fit for conventional FWI and both receiver extension strategies.*

	Conventional FWI	Static receiver extension	Time-dependent receiver extension (DP)
Forward simulation (s)	131.9	134.1	133.6
Inner loop (s)	-	21.6	42.6
Inner loop per receiver (s)	-	4.2×10^{-4}	8.4×10^{-4}
Adjoint simulation+gradient summation (s)	632	635.5	732.3
Total time required for a single gradient (s)	801.4	827.3	937.6
Extra cost w.r.t conventional FWI	-	3%	17%

Table 1: *CPU times for the different steps of computation. Eight OpenMP threads are used for each MPI task.*

In 3D, the number of grid points in each dimension is proportional to the inverse of the grid spacing, leading to a total grid size $N_{grid} \propto 1/h^3 \propto \omega^3$. Since the total number of time steps scales as $N_t \propto 1/\Delta t \propto \omega$, the cost of 3D FWI simulation scales as $\mathscr{O}(\omega^4)$.

The dynamic programming solver used for the receiver extension subproblem employs a tabulation approach. The point-wise cost is computed for all time steps and all possible relocalization positions

within a predetermined grid (varying from $-L$ to L with step Δs). The result is stored in an $N_{reloc} \times N_{Nyquist}$ array, where $N_{Nyquist}$ is the number of time steps sampled at the Nyquist frequency. The search bounds $\pm L$ are user-defined and fixed, with the relocalization step is $\Delta s \propto h \propto 1/\omega$, leading to $N_{reloc} \propto 2L/\Delta s \propto \omega$. The complexity of this approach is $\mathcal{O}(\omega^2)$. Please note that the full computation involves three steps: point-wise cost computation ($\mathcal{O}(\omega^2)$), cost accumulation over permissible paths ($\mathcal{O}(\omega^2)$), and backtracking ($\mathcal{O}(\omega)$). The complexity is therefore $\mathcal{O}(\omega^2)$.

This scaling analysis reveals a key advantage: while the cost of 3D FWI simulation scales as $\mathcal{O}(\omega^4)$, the receiver extension subproblem scales only as $\mathcal{O}(\omega^2)$. Consequently, the computational overhead of the extension strategy becomes negligible as the maximum frequency increases.

Conclusion and perspectives

We present an alternative extension strategy to mitigate the non-convexity of FWI, which is straightforward to implement in the time-domain. Thanks to the parsimonious parametrization and the efficient dynamic programming solver, the extension method scales as $\mathcal{O}(\omega^2)$, whereas 3D FWI scales as $\mathcal{O}(\omega^4)$.

We apply our method to an OBC dataset from the North Sea, starting the inversion in the 2-7 Hz frequency band. Unlike conventional FWI, which fails to correctly reconstruct the velocity model in this setting, our method yields satisfactory results with a manageable computational overhead.

Our findings warrant further investigation using a different field dataset. Another promising direction for future research would be extending the method to elastic FWI. Since the elastic wave equation accounts for a more complex wave phenomena, namely surface waves, S-waves, and converted waves, care must be taken to evaluate how the method behaves in these more complex settings.

Acknowledgements

The field data used in this study were provided by Aker BP and Inpex Idemitsu Norge. This study was partially funded by the SEISCOPE consortium (`http://seiscope2.osug.fr`), sponsored by Aker BP, DUG, EXXONMOBIL, GEOLINKS, JGI, PETROBRAS, SHEARWATER, SHELL, TOTALENERGIES and VIRIDIEN. This study was granted access to the HPC resources provided by the GRICAD infrastructure (https://gricad.univ-grenoble-alpes.fr), Marketing Partner Network (`https://partners.cray.com`) and CINES/IDRIS/TGCC under the allocation 046091 made by GENCI.

References

Barkved, O., Bærheim, A., Howe, D., Kommedal, J. and Nicol, G. [2003] Life of Field Seismic Implementation - Another "First at Valhall". In: *65th EAGE Workshop, Stavanger*.

Benziane, M., Brossier, R. and Metivier, L. [2025a] Time-Dependent Receiver Extension for FWI: A Dynamic Programming Approach. In: *86th EAGE Annual Conference & Exhibition*. European Association of Geoscientists & Engineers, 1–5.

Benziane, M., Brossier, R., Métivier, L. and Sambolian, S. [2025b] Time-dependent receiver extension for full-waveform inversion: An alternative extension method for cycle-skipping mitigation. *GEOPHYSICS*, **90**(6), R389–R412.

Bunks, C., Salek, F.M., Zaleski, S. and Chavent, G. [1995] Multiscale seismic waveform inversion. *Geophysics*, **60**(5), 1457–1473.

Hale, D. [2013] Dynamic warping of seismic images. *Geophysics*, **78**(2), S105–S115.

Métivier, L., Allain, A., Brossier, R., Mérigot, Q., Oudet, E. and Virieux, J. [2018] Optimal transport for mitigating cycle skipping in full waveform inversion: a graph space transform approach. *Geophysics*, **83**(5), R515–R540.

Métivier, L. and Brossier, R. [2022] Receiver-extension strategy for time-domain full-waveform inversion using a relocalization approach. *Geophysics*, **87**(1), R13–R33.

Métivier, L., Brossier, R., Górszczyk, A., Provenzano, G., Sambolian, S. and Tarayoun, A. [2025] High-resolution multi-parameter characterization of the subsurface using full waveform inversion on broadband data: application to the oceanic crust in the North sea using a dense Ocean Bottom Cable dataset. *Geophysical Journal International*, **in press**.

Operto, S., Gholami, A., Aghamiry, H., Guo, G., Beller, S., Aghazade, K., Mamfoumbi, F., Combe, L. and Ribodetti, A. [2023] Extending the search space of full-waveform inversion beyond the single-scattering Born approximation: A tutorial review. *GEOPHYSICS*, **88**(6), R671–R702.

Symes, W.W. [2008] Migration velocity analysis and waveform inversion. *Geophysical Prospecting*, **56**, 765–790.

Virieux, J. and Operto, S. [2009] An overview of full waveform inversion in exploration geophysics. *Geophysics*, **74**(6), WCC1–WCC26.

Warner, M. and Guasch, L. [2016] Adaptive waveform inversion: Theory. *Geophysics*, **81**(6), R429–R445.